Natural Convection in a Partitioned Trapezoidal Cavity Heated from the Side

F. Moukalled* and M. Darwish
Department of Mechanical Engineering
American University of Beirut
P.O.Box 11-0236
Riad El Solh, Beirut 1107 2020
Lebanon

ABSTRACT

Numerical results are reported for natural convection heat transfer in partially divided trapezoidal cavities representing industrial buildings. Two thermal boundary conditions are considered. In the first, the left short vertical wall is heated while the right long vertical wall is cooled (buoyancy assisting mode along the upper inclined surface of the cavity). In the second, the right long vertical wall is heated while the left short vertical wall is cooled (buoyancy opposing mode along the upper inclined surface of the cavity). The effects of Rayleigh number, Prandtl number, baffle height, and baffle location on the heat transfer are investigated. Results are displayed in terms of streamlines, isotherms, and local and average Nusselt number values. For both boundary conditions, predictions reveal a decrease in heat transfer in the presence of baffles with its rate generally increasing with increasing baffle height and Pr. For a given baffle height, higher decrease in heat transfer is generally obtained with baffles located close to the short vertical wall.

NOMENCLATURE

H_b baffle height

L_b baffle location

c_P specific heat of fluid

g gravitational acceleration

H height of the short vertical wall

H* height of the cavity at the location of the baffle

^{*} Corresponding Author email:memouk@aub.edu.lb

k thermal conductivity

Nu, Nu local and average Nusselt number

p,P dimensional and dimensionless pressure

Pr Prandtl number (= $\mu c_P / k$)

Ra Rayleigh number $(=g\beta(T_h - T_c)H^3/v\alpha)$

T dimensional temperature

u, U dimensional and dimensionless horizontal velocity component

v, V dimensional and dimensionless vertical velocity component

L width of the cavity

W_b baffle thickness

x, X dimensional and dimensionless coordinate along the horizontal direction

y, Y dimensional and dimensionless coordinate along the vertical direction

GREEK SYMBOLS

β coefficient of thermal expansion

μ viscosity

v kinematic viscosity (μ/ρ)

 θ dimensionless temperature

 θ_b dimensionless baffle temperature

ρ density

INTRODUCTION

Buoyancy-driven flows and transport processes in enclosures have been extensively analyzed in the literature. The bulk of the research in the area however, has concentrated on investigating natural convection in regular shaped enclosures (rectangular, cylindrical, annulus). By contrast, little attention has been given to the more challenging buoyancy-induced flows in enclosures of irregular geometry, which arise in many practical situations

(e.g. solar heating, solidification, nuclear waste disposal, etc...). The irregular boundaries in such enclosures coupled with the governing non-linear conservation equations result in fundamental solutions specific to the configurations at hand and difficult to envisage a priori from solutions obtained in regular enclosures. This paper deals with natural convection heat transfer in partially divided trapezoidal enclosures heated from the side.

Work on natural convection heat transfer in trapezoidal enclosures has been scarce. Iyican et al. [1,2] studied experimentally and numerically natural convection in an inclined trapezoidal cavity formed of parallel cylindrical cold top and hot bottom walls and plane adiabatic sidewalls. Lam et al. [3] reported similar results for a trapezoidal cavity composed of two vertical adiabatic sidewalls, a horizontal hot bottom wall, and an inclined cold top wall. Karyakin [4] investigated transient natural convection in a trapezoidal cavity with parallel top and bottom walls and inclined sidewalls. Lee [5,6] and Peric' [7] presented numerical results, up to a Rayleigh number of 10^5 , for natural convection in trapezoidal enclosures of horizontal bottom and top walls that are insulated and inclined sidewalls. Computations in the same geometry were carried out by Sadat and Salagnac [8] Ra ranging from 10^3 to $2x10^5$. Using the control volume method, further results in the same geometry were reported by Kuyper and Hoogendoorn [9] for $10^4 \le Ra \le 10^8$.

Studies related to buoyancy-induced heat transfer in partially divided trapezoidal cavities are limited to the ones reported in [10-12]. In [10,11], Moukalled and Acharya dealt with natural convection heat transfer in a partially divided trapezoidal cavity with partial dividers attached to the lower horizontal base [10] or the upper inclined surface [11] of the cavity. In [12] however, two offset baffles were employed. For all configurations, two boundary conditions representing summer-like and winter-like conditions were used. The current study differs from the previous ones in the geometry and boundary conditions. In [10-12], the cavity was symmetric in the x-direction (i.e. the symmetry boundary condition was applied along the right vertical boundary) and the upper inclined surface was either heated or cooled. In his

work, the cavity is half the one studied in [10-12] and the left vertical boundary is a wall boundary condition. In addition, the upper inclined surface is insulated. Similar to the work in [10], the baffle is attached to the lower horizontal base of the enclosure. As discussed in the extensive review on the subject presented by Ostrach [13], internal flows are more complex to predict than external flows due to the interaction between the boundary layer and core and that the core flow is very sensitive to the geometry and boundary conditions. This is inherent to all confined convection configurations. As such, any slight change in the geometry and/or boundary conditions may dramatically change the flow pattern within the cavity and justify the need to analyze this new configuration.

PHYSICAL MODEL AND GOVERNING EQUATIONS

The physical situation under consideration is schematically shown in Fig. 1(a). Solutions for natural convection within the cavity are obtained for two boundary conditions. In the first, the left short vertical wall of the cavity is maintained at the uniform hot temperature T_h and the right long vertical wall is maintained at the uniform cold temperature T_c . Since the height of the cavity increases in the direction of the rising fluid, this boundary condition corresponds to the buoyancy-assisting mode along the upper inclined plane. In the second, the left wall is cold (T_c) while the temperature of the right wall is T_h . This boundary condition corresponds to the buoyancy-opposing mode along the upper inclined plane. For both conditions, the effects of mounting a baffle to the lower horizontal plane of the cavity (Fig. 1(a)), on the amount of heat transferred across the cavity are analyzed.

In the configuration studied, the width of the cavity (L) is 4 times the height (H) of the short vertical wall. The inclination of the top of the cavity is fixed at 15 $^{\circ}$. Three baffle heights (H_b=H*/3, 2H*/3, and H* where H* is the height of the cavity at the location of baffle) and two baffle locations (L_b=L/3 and 2L/3) are considered. In all computations, the baffle thickness (W_b) is taken as W_b=L/20, to simulate a thin baffle.

The equations governing the flow and heat transfer are those expressing the conservation of mass, momentum, and energy. The flow is assumed to be laminar, steady, and two-dimensional with constant fluid properties, except for the induced variations in the body force term. The transport equations are non-dimensionalized using the following dimensionless variables:

$$X = \frac{x}{H}, Y = \frac{y}{H}, U = \frac{u}{v/H}, V = \frac{v}{v/H}, P = \frac{p + \rho gy}{\rho (v/H)^{2}}, \theta = \frac{T - T_{c}}{T_{h} - T_{c}}$$
(1)

With the stated assumptions and the Boussinesq approximation, the dimensionless governing transport equations of mass, momentum, and energy are, respectively,

$$\nabla.\mathbf{V} = 0 \tag{2}$$

$$\mathbf{V}.\nabla\mathbf{U} = -\mathbf{i}.\nabla\mathbf{P} + \nabla.(\nabla\mathbf{U}) \tag{3}$$

$$\mathbf{V}.\nabla \mathbf{V} = -\mathbf{j}.\nabla \mathbf{P} + \nabla.(\nabla \mathbf{V}) + \frac{\mathbf{Ra}.\theta}{\mathbf{Pr}} \tag{4}$$

$$\mathbf{V}.\nabla\theta = \frac{1}{\mathbf{P_r}}\nabla.(\nabla\theta) \tag{5}$$

In the baffle region, the only conservation equation needed is Laplace equation and is given by:

$$\nabla \cdot (\nabla \theta_{h}) = 0 \tag{6}$$

where θ_b denotes the non-dimensional temperature in the baffle. The energy balance at the baffle-air interface can be stated as

$$-\frac{1}{\mathbf{Pr}}(\mathbf{n}.\nabla\theta)_{i} = -\frac{\mathbf{k}_{r}}{\mathbf{Pr}}(\mathbf{n}.\nabla\theta_{b})_{i} \tag{7}$$

where h' is a unit vector normal to the baffle-air interface, the subscript i refers to the interface, and k_r is the ratio between the thermal conductivity of the baffle and the convective fluid.

The flow and thermal boundary conditions needed to solve the above system of equations are the no-slip condition on the enclosure walls, non-dimensional uniform temperatures of 1 and 0 along the hot and cold walls, and zero temperature gradient along the insulated inclined top

and horizontal bottom walls. This last boundary condition is numerically implemented by simply setting the fluid thermal conductivity at the insulated walls to zero.

SOLUTION PROCEDURE AND NUMERICAL ACCURACY

The SIMPLE algorithm of Patankar [14] along with collocated variables and the special Momentum Weighted Interpolation Method (MWIM) for the calculation of the mass fluxes across the control volume faces [15] are employed to arrive at the solution to the coupled system of equations governing the flow and temperature fields (Eqs. (2)-(6)). In this procedure, the solution domain is subdivided into a number of control volumes with a grid point located at the center of each cell (Fig. 1(b)). First integrating the equations over each control volume and then using Green's theorem to replace the volume integral by the surface integral obtain the discretized forms. With suitable profile interpolation in each coordinate direction (the third order SMART scheme [16] is used and applied within the context of the NVSF methodology [17]) for the variables whose values are unknown on the control volume faces, a system of algebraic equation results that can be solved iteratively using a line-by-line Thomas algorithm. Pressure-velocity coupling is resolved through a guess-and-correct procedure similar to that described by Patankar [14]. Moreover, the presence of the baffle in the calculation domain is accounted for by the special treatment suggested by Patankar [14]. With this approach, the baffle region is treated as an infinitely viscous fluid (numerically specified as a very large value) with a non-dimensional thermal conductivity corresponding to that of the baffle. This procedure leads to zero velocities in the baffle region, and the energy equation reduces to that of the Laplace heat conduction equation. Because a conservative scheme is used, arranging the control volume face to coincide with the divider interface ensures energy balance at the baffle-air interface and forces equation (7) to be implicitly satisfied.

All calculations have been done on a 68x62 non-uniform grid with the grid points clustered more closely along all solid boundaries (Fig. 1(c)). This choice was based on a number of preliminary calculations with successively finer grids. The accuracy of the calculations was verified by comparing computed profiles of velocity, temperature, and local Nusselt number using the 68x62 non-uniform grid with those obtained on a 130x130 nearly uniform grid. The maximum difference in the two solutions was smaller than 0.113%.

RESULTS AND DISCUSSION

The governing parameters in the problem are the Prandtl number (Pr), the Rayleigh number (Ra), the conductivity ratio (k_r), the baffle height (H_b), and the baffle location (L_b). The conductivity ratio is fixed at 2 to simulate a poorly conducting divider. Moreover, for both boundary conditions predictions are obtained for three Prandtl number values (Pr=0.7, 10, and 130), three baffle heights ($H_b=H^*/3$, $2H^*/3$, and H^*), two baffle locations ($L_b=L/3$ and 2L/3), and Rayleigh number values varying between 10^3 and 10^6 . Results are presented in the form of representative streamlines, isotherms, and local and average Nusselt number values.

BUOYANCY-ASSISTING FLOW ALONG THE TOP INCLINED SURFACE OF THE ENCLOSURE

Streamlines and isotherms

Streamline and isotherm plots, for Pr=0.7, are shown in Figs. 2-5. In the baffle-free enclosure (Fig. 2), the flow consists of a recirculating eddy rotating clockwise, indicating that the fluid filling the cavity is moving up along both the left heated vertical wall and the top insulated inclined surface, down along the cooled right vertical wall, and horizontally to the left along the insulated base of the trapezoidal enclosure. At low Ra values, the eye of the recirculation is close to the vertical cold wall of the enclosure, where the largest velocities are located (Figs. 2(a) and 2(b)). As Ra increases (Figs. 2(c) and 2(d)), the eye moves away from the cold wall towards the middle of the domain and upward towards the top inclined plane of the

cavity. In addition, at the highest Ra value (Ra=10⁶), the flow separates near the lower right corner of the cavity. This behavior is opposite to the one reported in [11].

At low Ra (Ra=10³), isotherms are uniformly distributed over the domain (Fig. 2(e)), implying weak convection effects. As Ra increases, isotherms become more distorted and stratification effects in the enclosure increase (compare Figs. 2(e)-2(h)) indicating dominant convection. In addition, the boundary layer-type flow along the hot and cold wall becomes clearer.

The effects of baffles on flow patterns and temperature distributions are depicted in Figure 3 for L_b=L/3, H_b=2H*/3 and in Figure 4 for L_b=2L/3, H_b=2H*/3. Streamlines in Figure 3 indicate that at the lowest Ra presented (Ra=10³), the recirculating flow exhibits two vortices communicating through a very thin overall rotating eddy (Figure 3(a)). These two vortices rotate in the clockwise direction. As Ra increases, communication between the vortices increases until at Ra=106 the two vortices merge into one (Figure 2(d)). Moreover, with increasing values of Ra, the flow between the divider and the cold wall becomes weaker as compared to the region between the divider and the hot wall. The colder fluid tends to stagnate in the lower right hand section of the cavity between the divider and the cold wall, resulting in a thermally stratified region and inhibiting the penetration of the warmer fluid from the cavity left hand section. As a consequence, a jet-like flow directed from the cold wall to the baffle tip is observed at Ra=10⁶. Even though the flow in the lower right hand portion of the domain is weak, the stratification effects are not strong enough to cause separation. Isotherms presented in Figures 3(e)-3(h) reflect the above described flow patterns. At low Ra, variations in temperature are almost uniform over the domain, indicating dominant conduction heat transfer mode. As Ra increases, convection is promoted, and isotherms become more distorted.

The effects of positioning the baffle closer to the cold vertical wall on the velocity and temperature fields are depicted in Figure 4 ($L_b=2L/3$, $H_b=2H^*/3$). At low Ra values (Figures

4(a) and 4(b)), the flow structure is qualitatively similar to that presented in Figures 3(a) and 3(b). As Ra values increase (Figures 4(c) and 4(d)), a more pronounced thermally stratified zone develops in the baffle-cold wall region as compared to the configuration in which the baffle is closer to the hot wall (Figures 3(c) and 3(d)). This thermally stratified region prevents the bulk of the fluid descending along the cold wall from penetrating the region. Instead, the fluid tends to flow directly around the divider towards the hot wall. The near stagnant fluid in the divider-cold wall region reduces the effective flow area in the cavity and is expected to reduce the total heat transfer rate. Moreover, at Ra=10⁶, the flow along the insulated base of the cavity to the right hand side of the baffle separates. The highly thermally stratified fluid descending the baffle that is not able to negotiate towards the left hot wall of the enclosure causes this separation. The above described behavior is further exemplified by the isotherm plots presented in Figures 4(e)-4(h). At Ra=10³ (Figure 4(e)) stratification effects are small and distribution of isotherms is more or less uniform. As Ra increases, isotherms become more distorted (Figures 4(f)-4(h)) and stratification effects are promoted (Figures 4(g) and 4(h)).

The effects of baffle height on the hydrodynamic and thermal fields are presented in Figure 5 in an enclosure with a divider located at L_b =L/3 and for Ra= 10^5 . Streamlines and isotherms are displayed for four different baffle heights of H_b =0, $H^*/3$, $2H^*/3$, and H^* . As the baffle height is increased, a weaker flow is observed between the divider and the cold wall, compared to the region between the divider and the hot wall. A small recirculation bubble is noted behind the divider at H_b = $H^*/3$ (Figure 5(b)). A similar recirculation bubble was reported by Acharya and Jetli [18] in their study of natural convection in a partially divided square box for the same value of baffle height with the recirculation eddy disappearing for H_b = $2H^*/3$, which is the case here. Moreover, separation or splitting of the clockwise rotating eddy is noted behind the divider at H_b = $2H^*/3$ (Figure 5(c)). For the same baffle height in a partially divided square box, Acharya and Jetli [18] reported similar findings. For a fully

partitioned enclosure (Figure 5(d)), two similar clockwise rotating eddies are noticed with the one between the cold wall and the baffle being of lower strength. Isotherms presented in Figs. 5(e)-5(h) are in line with above findings.

Nusselt numbers

The local and average Nusselt numbers along the hot or cold wall are computed from:

$$Nu = h\lambda/k \qquad \overline{Nu} = \frac{1}{\lambda} \int_{0}^{\lambda} Nu dx \qquad (8)$$

where I is the height of the hot or cold wall. Based on this definition, the average Nusselt numbers along both walls are equal. Moreover, the heat transfer coefficient h is defined as

$$\mathfrak{E} = hA(T_h - T_c) = -kA\frac{dT}{dx} \Rightarrow h = -\frac{k}{H}\frac{d\theta}{dX} \tag{9}$$

Local Nusselt number variations (Nu) along the hot and cold sidewalls are presented in Figure 6. Values are plotted as a function of Y/Y_{max} where $Y_{max} = \lambda$ is the height of the hot or cold wall.

The Nu distributions along the hot and cold walls in a baffle free enclosure are compared in Figures 6(a) and 6(b) respectively, against profiles obtained in a partitioned enclosure of baffle height $H_b=2H^*/3$ located at $L_b=L/3$. As shown, the Nu levels increase with increasing Ra indicating higher convection contribution. Both the hot and cold wall profiles have a sharp peak, which is more pronounced at higher Ra values, occurring at the lower and upper sections of the walls, respectively, at the points where the cold and warm flows impinge directly onto them. The peak on the cold wall is sharper than the one on the hot wall due to the aiding effects of buoyancy along the upper inclined plane of the enclosure, which further increases the velocity of the hot fluid before impinging on the cold wall. At all Ra values, the profiles in a partitioned enclosure are below their counterparts in a baffle free enclosure implying, as expected, a decrease in convection heat transfer. At Ra= 10^6 , this decrease in heat transfer along the cold wall (Figure 6(b)) is seen to be concentrated in the lower portion

of the enclosure due to the flow stratification in that region caused by the partial divider. The effects of baffle height on Nu distributions along the hot and cold walls are depicted in Figures 6(c) and 6(d), respectively, in an enclosure with a baffle located at L_b=L/3 and for an Ra value of 10⁵. As shown, the trends of variations in Nu along both walls are similar for all baffle heights with the level of Nu decreasing with increasing H_b. The Nu estimates in an enclosure with a baffle of height H_b=H*/3 are slightly lower than values in a baffle free enclosure. However, notable decrease is achieved as the baffle height is increased. This is further revealed by the average Nusselt number values displayed in Table 1 which show, at high Ra values, a significant reduction in heat transfer as the baffle height is increased. At the lowest Ra considered (10³) and for all Pr values, the \overline{Nu} values are seen to minimize at a certain baffle height. Since convection contribution to total heat transfer is low at low Ra values, the increase in conduction within the enclosure as the baffle height is increased overwhelms the decrease in convection and the net effect is an increase in total heat transfer. For a given baffle height, the total heat transfer increases with increasing Ra values due to an increase in convection heat transfer. Ratios of the partially divided enclosure Nusselt numbers to those of an open enclosure at the same Rayleigh number (Pr=0.7) reveals that at the higher Rayleigh numbers, the percentage reduction in heat transfer varies from about 3.96% at H_b=H*/3 to 66.6% at H_b=H* when the baffle is located at L_b=L/3, and from about 5.56% at $H_b=H^*/3$ to 61.9% at $H_b=H^*$ when $L_b=2L/3$. Moreover, \overline{Nu} increases with increasing Pr due to a decrease in the thermal boundary layer thickness along the walls with a consequent increase in the temperature gradient. Moreover, the rate of increase increases with increasing Rayleigh number and decreases with increasing Pr.

BUOYANCY-OPPOSING FLOW ALONG THE TOP INCLINED SURFACE OF THE ENCLOSURE

Streamlines and isotherms

Representative flow patterns and temperature distributions, for Pr=0.7, are depicted in Figs. 7-10.

In the absence of baffles (Fig. 7), the flow in the enclosure is composed of a single counterclockwise rotating cell. At low Ra, the eye of the recirculation is close to the vertical hot wall of the enclosure (Figs. 7(a) and 7(b)). As Ra increases (Figs. 7(c) and 7(d)), the eye elongates and separates into two vortices close to the hot and cold walls, respectively.

At low Ra (Ra=10³), isotherms are uniformly distributed over the domain (Fig. 7(e)), implying weak convection effects. As Ra increases, similar to the buoyancy assisting case, isotherms become more distorted and mixing effects in the enclosure increase (compare Figs. 7(e)-7(h)) indicating dominant convection heat transfer mode. In addition, the boundary layer-type flow along the hot and cold wall becomes clearer.

Streamline and isotherm maps for a partitioned enclosure are depicted in Figs. 8 through 10. In difference with the buoyancy-aiding situation (Figs. 3 and 4), streamlines indicate that the flow moves in the counterclockwise direction and the jet-like flow is less apparent with the depth of its penetration into the left-hand portion of the domain being small (compare streamline plots in Figs. 8 and 9 against those presented in Figs. 3 and 4). This is caused by buoyancy, which slows down the flow descending along the inclined upper surface of the cavity. Moreover, the flow neither separates nor stagnates on either side behind the divider. Furthermore, isotherms reveal high stratification levels on the top right hand side of the domain where the hot rising fluid has to descend along the top inclined surface. This behavior is opposite to what happens in the buoyancy-aiding situation where thermal stratification was pronounced in the lower right hand portion of the domain. By comparing results in Fig. 8 against those reported in Fig. 9 it can be inferred that placing the divider close to the hot wall has little effect on the global flow structure and thermal stratification in the enclosure. Figure

10 reveals the effects of baffle height in an enclosure with a divider located at L_b =L/3 and for Ra= 10^5 . As the baffle height is increased, the flow becomes weaker and a decrease in convection effects is observed which is manifested by a lighter clustering of isotherms along the walls.

Nusselt numbers

The local and average Nusselt number values along the hot and cold walls are computed using Eq. (8). The effects on heat transfer of partitioning the cavity can be assessed by a direct comparison between the Nu distributions along the hot and cold walls in a nonpartitioned and partitioned enclosures (H_b=2H*/3, L_b=L/3) that are displayed in Figures 11(a)-11(d). The decrease in heat transfer in the presence of baffles can easily be depicted from the profiles presented in Figures 11(a) and 11(b) where the Nu levels are seen to be higher in a baffle free enclosure especially at high Ra values where convection is the dominant heat transfer mode. As the fluid flows down the left cold wall, its temperature decreases causing a decrease in heat transfer and consequently in Nu (Fig. 11(a)). The high Nu value near Y/Y_{max}=1 (Fig. 11 (a)), is due to the large temperature difference between the hot fluid and the cold wall. As the fluid moves up along the hot wall its temperature increases and the temperature difference between the fluid and the hot wall decreases. This results in a decrease in Nu values as depicted in Fig. 11(b). The peak at the leading edge of the hot wall is caused by the impingement of the cold fluid there while trying to negotiate the corner. Moreover, Figs. 11(c) and 11(d) (Ra=10⁵, L_b=L/3) reveal that the effect of increasing the baffle height is to decrease the Nu values along the hot and cold walls and consequently to reduce heat transfer.

The average Nusselt number values for all cases studied are displayed in Table 2. Predictions indicate a decrease in heat transfer in the presence of baffles. For Ra= 10^3 and for all Pr values, the increase in conduction overwhelms the decrease in convection as the baffle height is increased and results in an optimum baffle height for which $\overline{\text{Nu}}$ is minimum. For Ra $\geq 10^4$

however, the decrease in heat transfer increases with increasing baffle height for all Pr values considered. Moreover, for a given baffle height, the total heat transfer increases with increasing Ra due to an increase in convection heat transfer. At Ra=10⁶ and Pr=0.7, the percent reduction in heat transfer varies from about 14.423% at $H_b=H^*/3$ to 63.74% at $H_b=H^*$ when the baffle is located at $L_b=L/3$, and from about 20.27% at $H_b=H^*/3$ to 60.44% at $H_b=H^*$ when $L_b=2L/3$. As in the buoyancy-assisting case, \overline{Nu} increases with increasing Pr due to a decrease in the thermal boundary layer thickness along the walls with a consequent increase in the temperature gradient.

CLOSING REMARKS

Natural convection in a partitioned trapezoidal cavity heated from the side has been studied numerically. In particular, the effects of Rayleigh number, Prandtl number, baffle height, and baffle location on heat transfer are investigated for two boundary conditions representing buoyancy assisting and buoyancy opposing modes along the upper inclined surface of the cavity. For both boundary conditions, convection contribution to total heat transfer is found to increase with increasing Rayleigh number. The presence of baffles decreases heat transfer with its rate increasing with increasing both Pr and H_b. For the cases considered, a decrease in heat transfer as high as 70% was achieved.

ACKNOWLEDGMENTS

The financial support provided by the University Research Board of the American University of Beirut through Grant No. 1799-60-73616 is gratefully acknowledged.

REFERENCES

 Iyican, L., Bayazitoglu, Y., and Witte, L.," An Analytical Study of Natural Convective Heat Transfer within a Trapezoidal Enclosure", J. of Heat Transfer, vol. 102, pp. 640-647, 1980.

- 2. Iyican, L., Witte, L.C., and Bayazitoglu, Y.," An Experimental Study of Natural Convection in Trapezoidal Enclosures", J. of Heat Transfer, vol. 102, pp. 648-653, 1980.
- 3. Lam, S.W., Gani, R., and Simons, J.G.," Experimental and Numerical Studies of Natural Convection in Trapezoidal Cavities", J. of Heat Transfer, vol. 111, pp. 372-377, 1989.
- 4. Karyakin, Y.E." Transient Natural Convection in Prismatic Enclosures of Arbitrary cross-section", Int. J. Heat Mass Transfer, vol. 32, No. 6, pp. 1095-1103, 1989.
- 5. Lee, T.S.," Numerical Experiments with Fluid Convection in Tilted Nonrectangular Enclosures," NHT, Part A, vol. 19, pp. 487-499, 1991.
- 6. Lee, T.S.,"Computational and Experimental Studies of Convective Fluid Motion and Heat Transfer in Inclined non-rectangular enclosures," International Journal of Heat and Fluid Flow, vol.5, pp. 29-36, 1984.
- 7. Peric', M.,"Natural Convection in Trapezoidal Cavities," NHT, Part A, vol. 24, pp. 213-219, 1993.
- 8. Sadat, H. and Salagnac, P.," Further results for Laminar Natural Convection in a Two-dimensional Trapezoidal Enclosure," NHT, Part A, vol. 27, pp. 451-459, 1995.
- 9. Kuyper, R.A. and Hoogendoorn, C.J.," Laminar Natural Convection Flow in Trapezoidal Enclosures," NHT, Part A, vol. 28, pp. 55-67, 1995.
- 10. Moukalled, F. and Acharya, S.," Buoyancy-Induced Heat Transfer in Partially Divided Trapezoidal Cavities," NHT, Part A, vol. 32, pp. 787-810, 1997.
- Moukalled, F. and Acharya, S.," Natural Convection in Trapezoidal Cavities with Baffles Mounted on The Upper Inclined Surfaces," NHT, Par A: vol. 37, No. 6, pp.545-565, 2000.
- 12. Moukalled, F. and Acharya, S. "Natural Convection in a Trapezoidal Enclosure with Offset Baffle," AIAA Journal of Thermophysics and Heat Transfer, vol. 15, No. 2, pp. 212-218, 2001.

- 13. Ostrach, S., "Natural Convection in Enclosures," J. of Heat Transfer, vol. 110, pp. 1175-1190, 1988.
- 14. Patankar, S.V., Numerical Heat Transfer and Fluid Flow, New York, Hemisphere Publishing Corporation, 1980.
- 15. Peric, M., "A Finite Volume Method for the Prediction of Three Dimensional Fluid Flow in Complex Ducts," Ph.D. Thesis, Imperial College, Mech. Eng. Department, London, 1985.
- Gaskell, P.H. and Lau, A.K.C., "Curvature compensated Convective Transport: SMART, a new boundedness preserving transport algorithm," Int. J. Num. Meth. Fluids, vol. 8, pp. 617-641, 1988.
- 17. Darwish, M. and Moukalled, F.," Normalized Variable and Space Formulation Methodology For High-Resolution Schemes," NHT, Part B, vol. 26, pp. 79-96, 1994.
- 18. Acharya, S. and Jetli, R.,"Heat Transfer Due to Buoyancy in a Partially Divided Square Box," International Journal of Heat and Mass Transfer, vol. 33, pp. 931-942, 1990.

FIGURE CAPTIONS

- Fig. 1 (a) Physical domain; (b) computational domain and an illustrative grid network; (c) a typical control volume.
- Fig. 2 Streamline and isotherm plots in a non-partitioned cavity for the buoyancy assisting boundary condition.
- Fig. 3 Streamline and isotherm plots ($H_b=2H^*/3$, $L_b=L/3$) for the buoyancy assisting boundary condition.
- Fig. 4 Streamline and isotherm plots ($H_b=2H*/3$, $L_b=2L/3$) for the buoyancy assisting boundary condition.
- Fig. 5 Streamline and isotherm plots ($Ra=10^5$, $L_b=L/3$) at different H_b for the buoyancy assisting boundary condition.

- Fig. 6 Local Nusselt number distribution along (a,c) the hot and (b,d) cold walls for the buoyancy assisting boundary condition.
- Fig. 7 Streamline and isotherm plots in a non-partitioned cavity for the buoyancy opposing boundary condition.
- Fig. 8 Streamline and isotherm plots ($H_b=2H^*/3$, $L_b=L/3$) for the buoyancy opposing boundary condition.
- Fig. 9 Streamline and isotherm plots ($H_b=2H^*/3$, $L_b=2L/3$) for the buoyancy opposing boundary condition.
- Fig. 10 Streamline and isotherm plots ($Ra=10^5$, $L_b=L/3$) at different H_b for the buoyancy opposing boundary condition.
- Fig. 11 Local Nusselt number distribution along (a,c) the hot and (b,d) cold walls for the buoyancy opposing boundary condition.

Table 1 Average Nusselt number values (\overline{Nu}) for hot left (short) wall and cold right (tall) wall (Buoyancy assisting boundary condition)

	No baffle	$H_b = H^*/3$	$H_b = 2H^*/3$	$H_b = H^*$	$H_b = H^*/3$	$H_b = 2H^*/3$	$H_b = H^*$				
Ra		$L_b=L/3$			$L_b = 2L/3$						
Pr=0.7											
103	0.715	0.546	0.503	0.507	0.567	0.49	0.492				
104	2.48	2.142	1.131	1.108	2.256	1.305	1.224				
105	5.476	5.303	3.557	2.136	5.166	3.945	2.404				
106	10.925	10.492	9.106	3.648	10.317	8.57	4.162				
Pr=10											
103	0.719	0.547	0.504	0.508	0.569	0.4906	0.493				
104	2.666	2.261	1.171	1.142	2.396	1.369	1.258				
105	6.102	5.86	4.064	2.2355	5.709	4.431	2.529				
106	12.077	11.5249	10.33	3.791	11.201	9.559	4.342				
Pr=130											
103	0.719	0.5475	0.504	0.508	0.5692	0.4906	0.493				
104	2.67	2.263	1.172	1.143	2.4	1.371	1.259				
105	6.125	5.88	4.076	2.237	5.7254	4.443	2.532				
106	12.142	11.58	10.37	3.7954	11.259	9.595	4.347				

Table 2 Average Nusselt number values (\overline{Nu}) for cold left (short) wall and hot right (tall) wall (Buoyancy opposing boundary condition)

	No baffle	$H_b = H^*/3$	$H_b = 2H^*/3$	$H_b = H^*$	$H_b = H^*/3$	$H_b = 2H^*/3$	$H_b = H^*$				
Ra		$L_b=L/3$			$L_b = 2L/3$						
Pr=0.7											
103	0.6153	0.508	0.479	0.484	0.504	0.464	0.467				
104	1.922	1.475	0.988	0.985	1.551	1.072	1.051				
105	4.431	3.678	2.1456	1.89	3.564	2.294	2.062				
106	8.84	7.565	4.15	3.205	7.048	4.066	3.497				
Pr=10											
103	0.617	0.509	0.48	0.4844	0.504	0.4643	0.4668				
104	1.986	1.51	1.001	0.998	1.5713	1.084	1.0626				
105	4.686	3.91	2.2	1.926	3.74	2.354	2.109				
106	9.358	8.047	4.3604	3.266	7.478	4.199	3.575				
Pr=130											
103	0.617	0.509	4.8	0.4845	0.504	0.464	0.4668				
104	1.988	1.511	1.001	0.998	1.57	1.084	1.063				
105	4.694	3.914	2.201	1.9266	3.742	2.355	2.11				
106	9.375	8.057	4.367	3.2685	7.485	4.202	3.578				

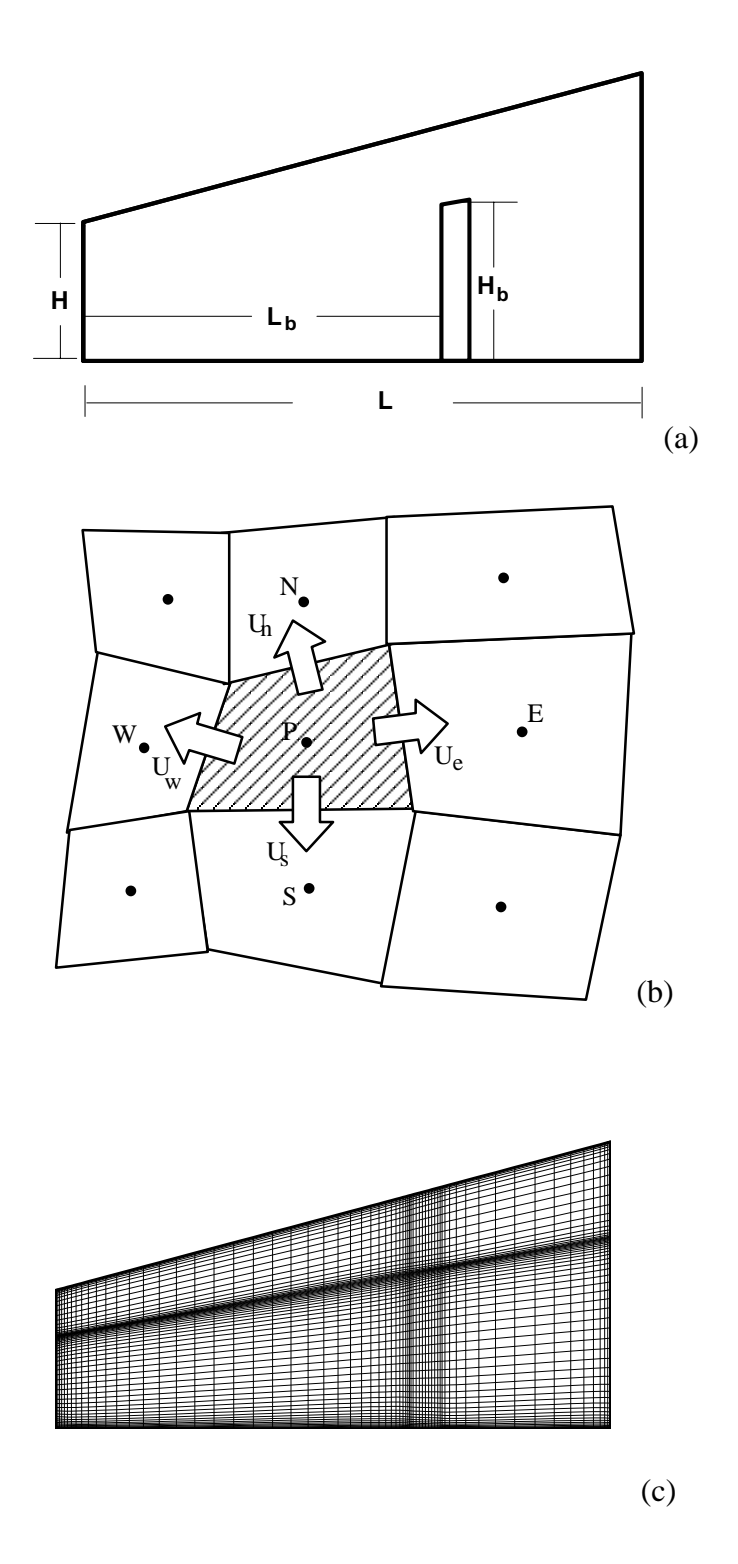


Fig. 1 (a) physical situation, (b) Control volume, (c) an illustrative grid network used.

Streamlines

Isotherms

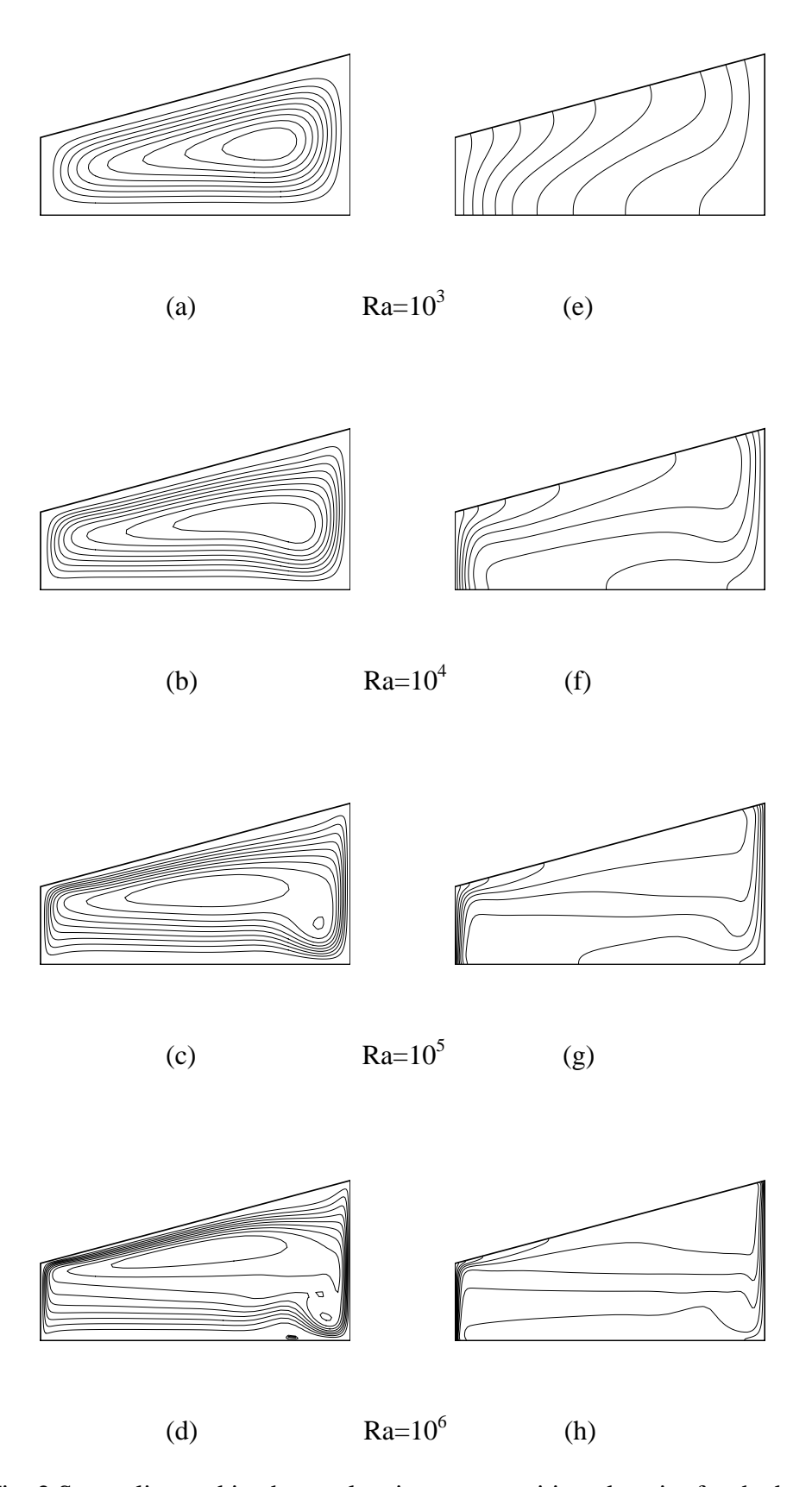


Fig. 2 Streamline and isotherm plots in a non-partitioned cavity for the buoyancy assisting boundary condition.

Streamlines Isotherms

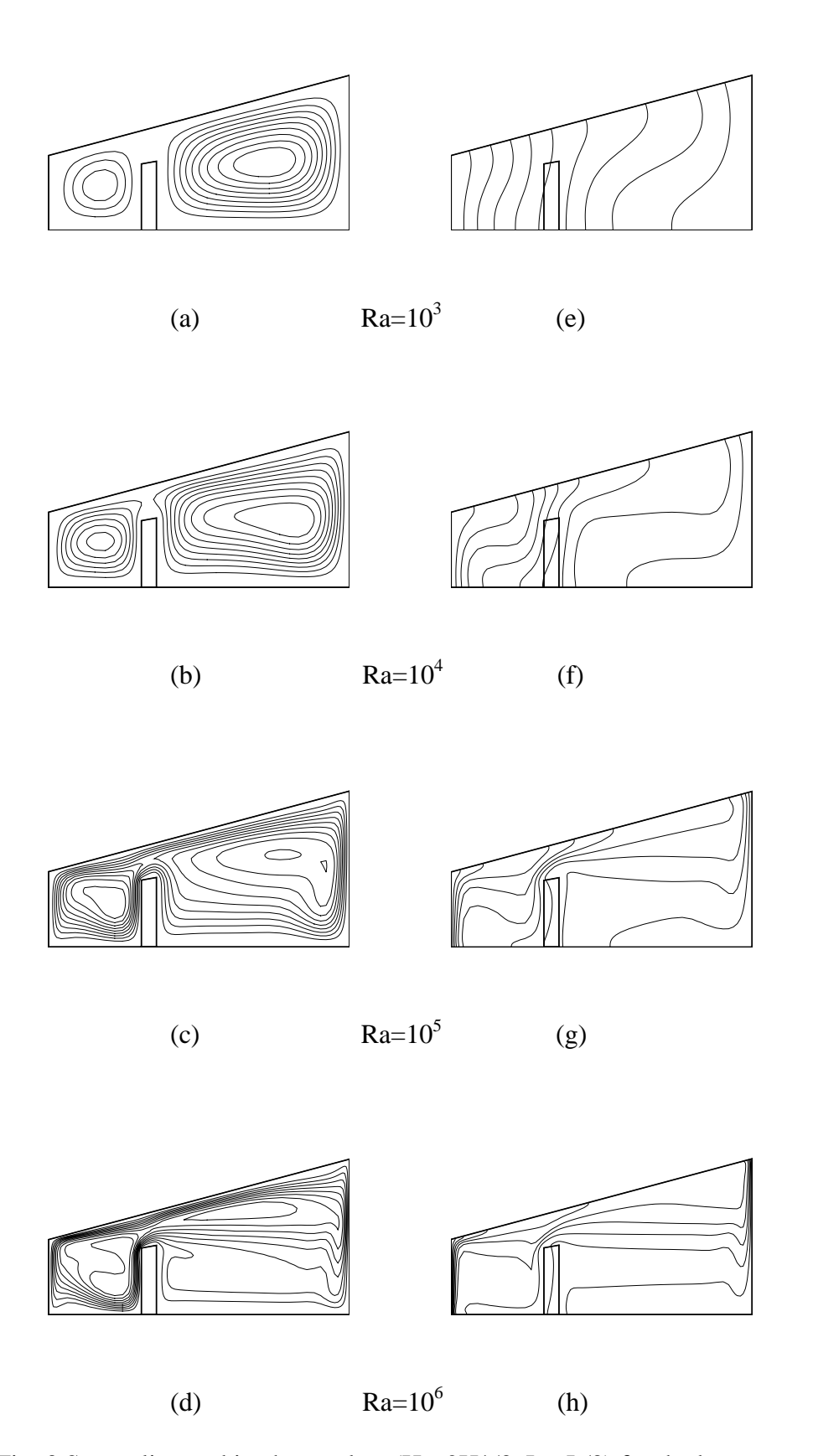
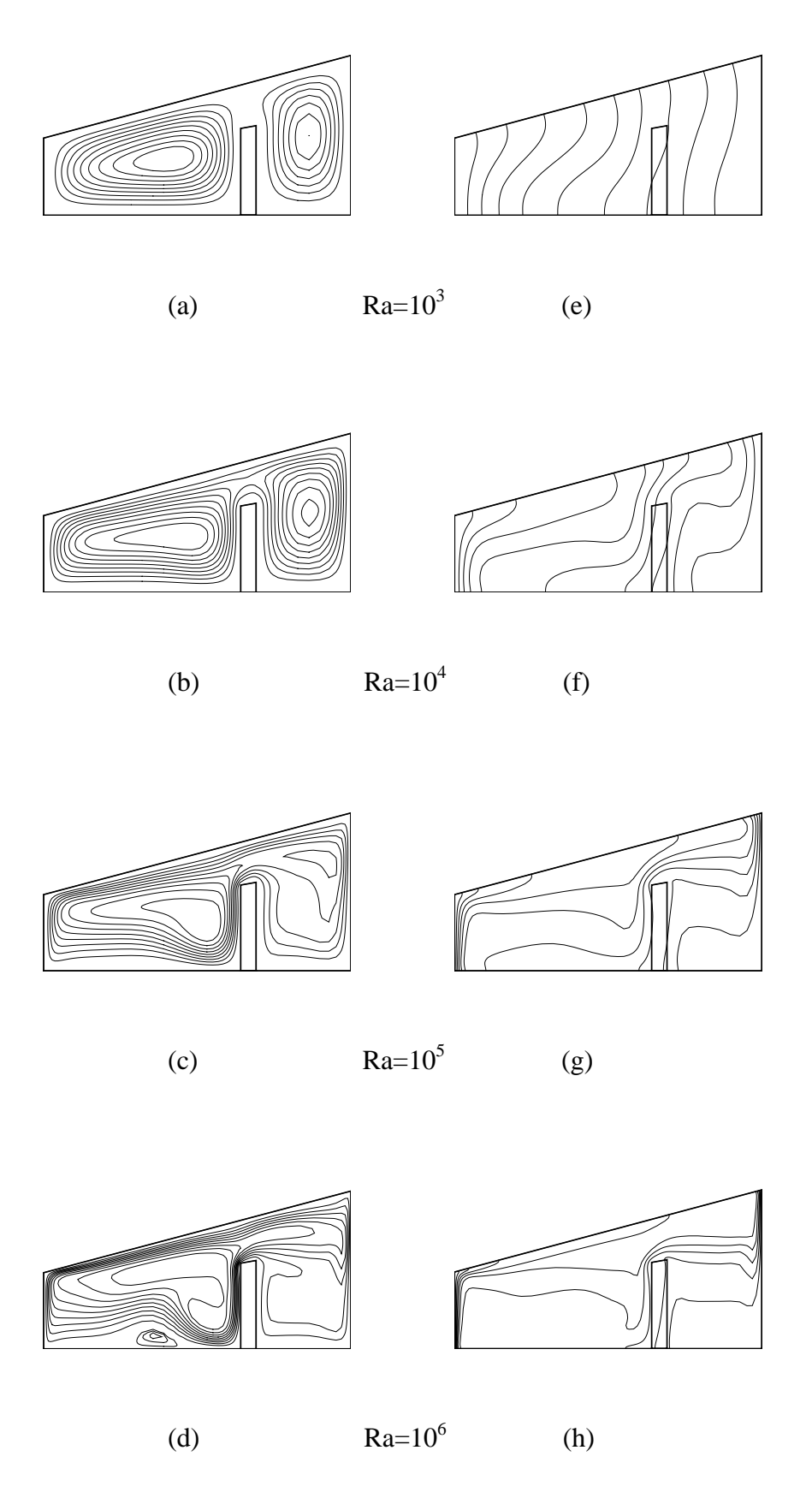


Fig. 3 Streamline and isotherm plots ($H_b=2H^*/3$, $L_b=L/3$) for the buoyancy assisting boundary condition.

Streamlines

Isotherms



 $Fig.~4~Streamline~and~isotherm~plots~(H_b=2H^*/3,~L_b=2L/3)~for~the~buoyancy~assisting\\$ boundary condition

Streamlines

Isotherms

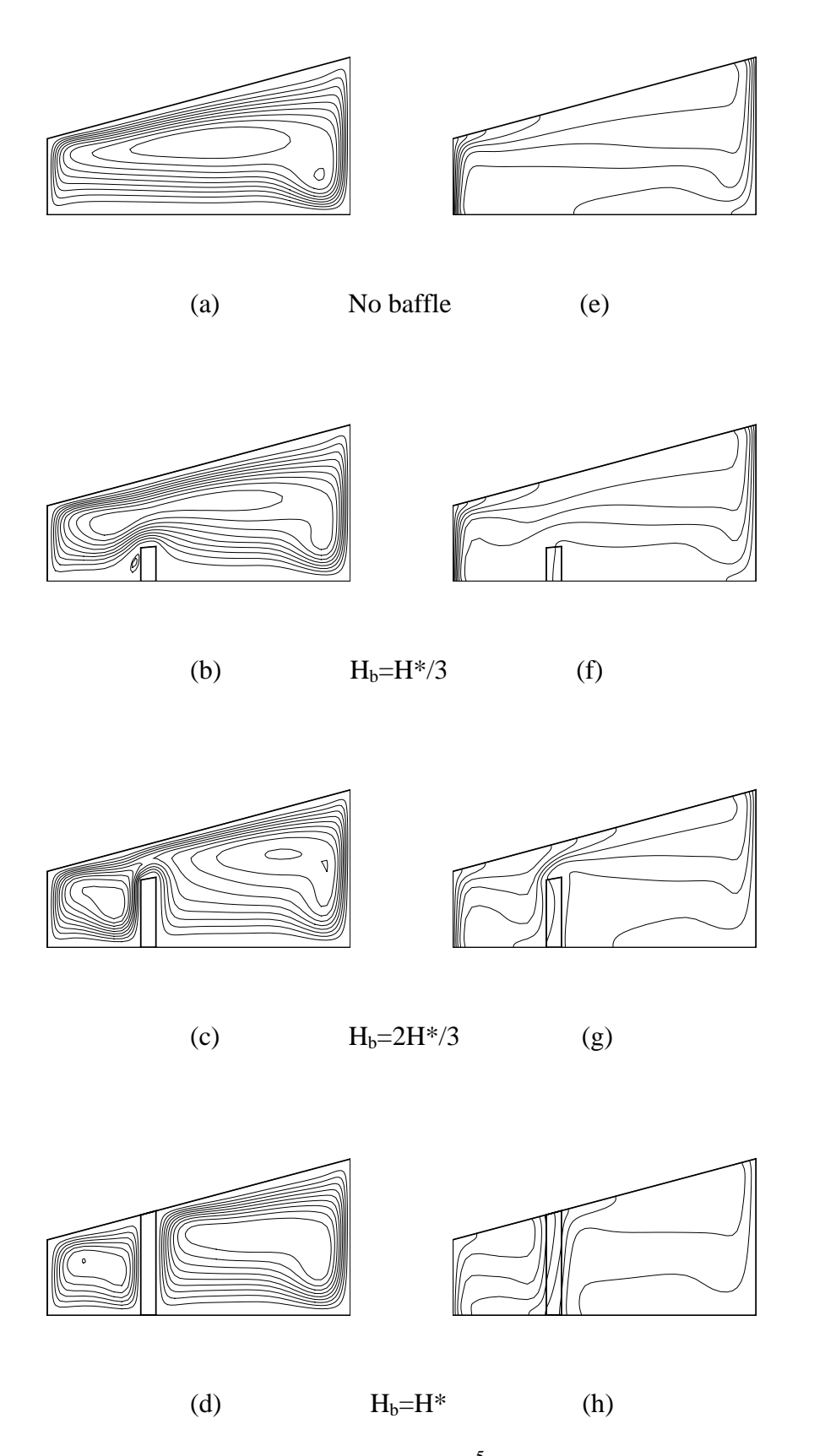
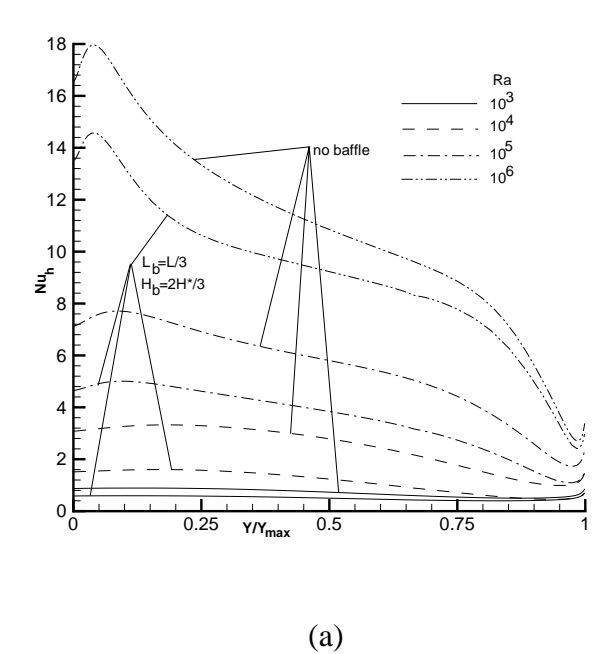
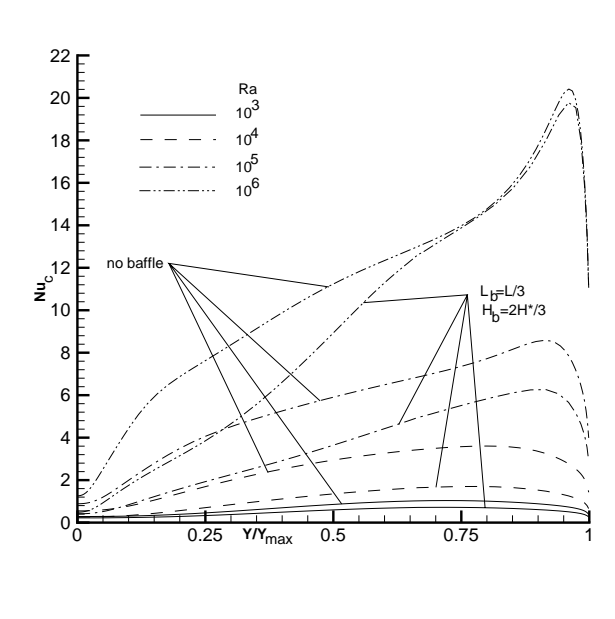
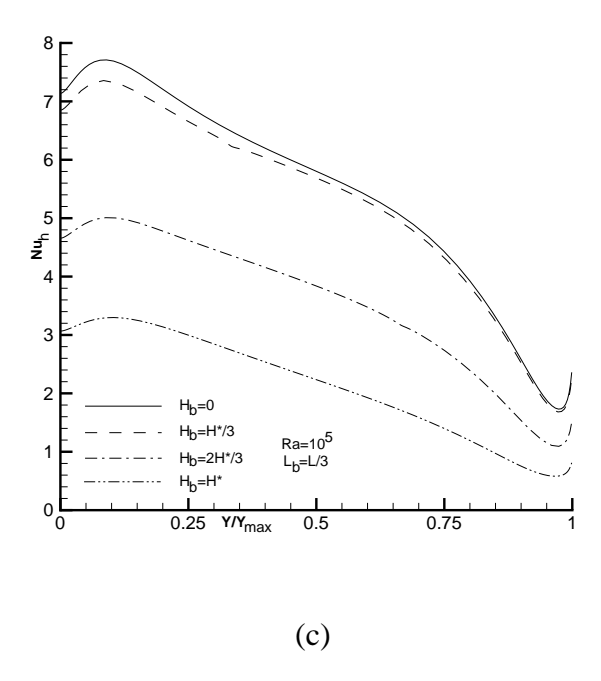


Fig. 5 Streamline and isotherm plots (Ra= 10^5 , L_b =L/3) at different H_b for the buoyancy assisting boundary condition.





(b)



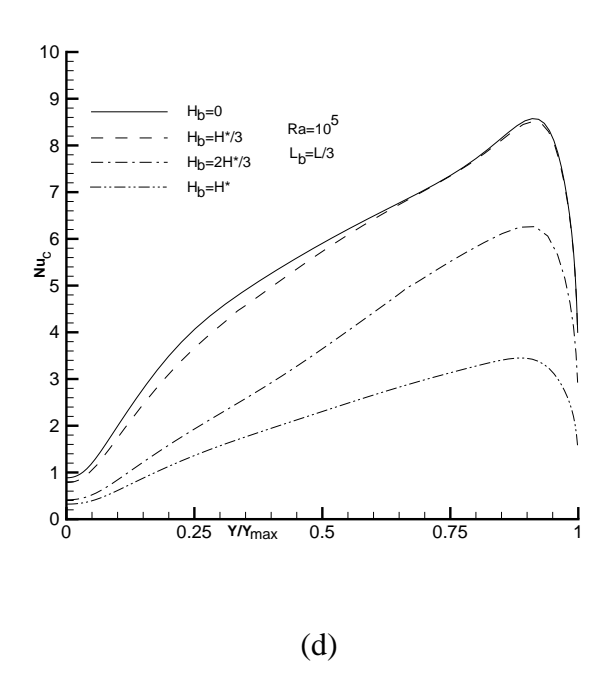


Fig. 6 Local Nusselt number distribution along (a,c) the hot and (b,d) cold walls for the buoyancy assisting boundary condition.

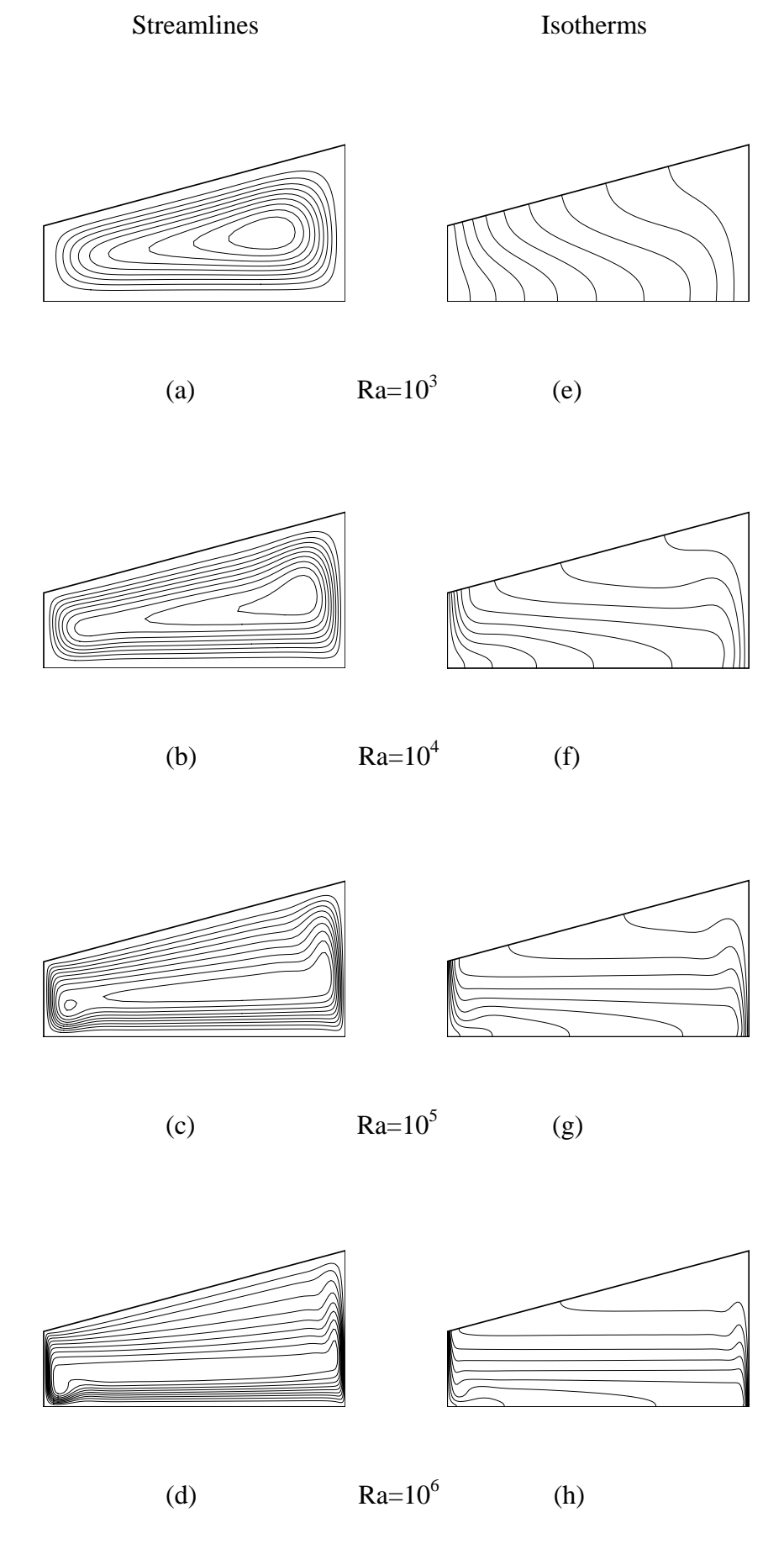


Fig. 7 Streamline and isotherm plots in a non-partitioned cavity for the buoyancy opposing boundary condition.

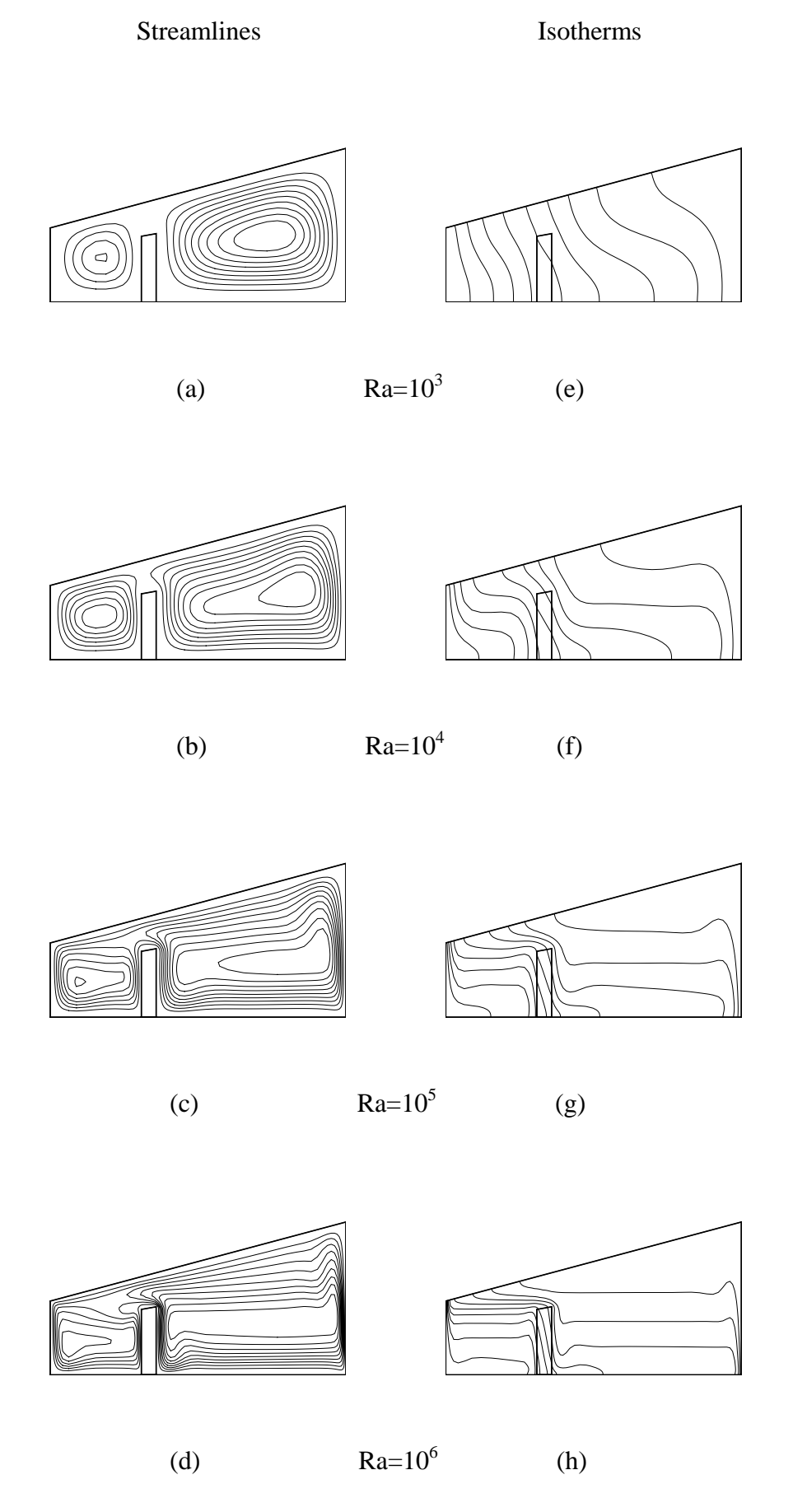


Fig. 8 Streamline and isotherm plots ($H_b=2H^*/3$, $L_b=L/3$) for the buoyancy opposing boundary condition.

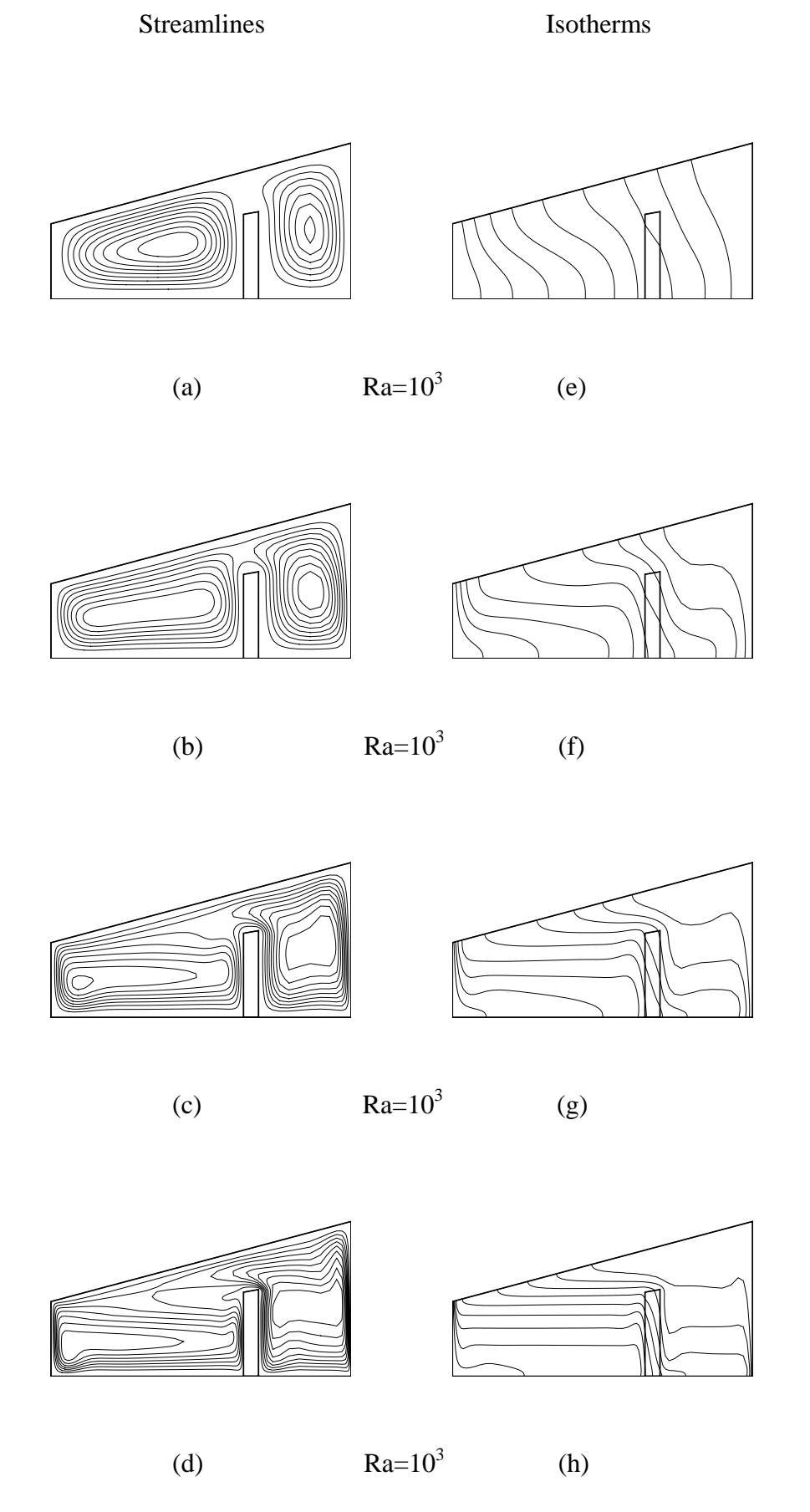


Fig. 9 Streamline and isotherm plots ($H_b=2H^*/3$, $L_b=2L/3$) for the buoyancy opposing boundary condition.

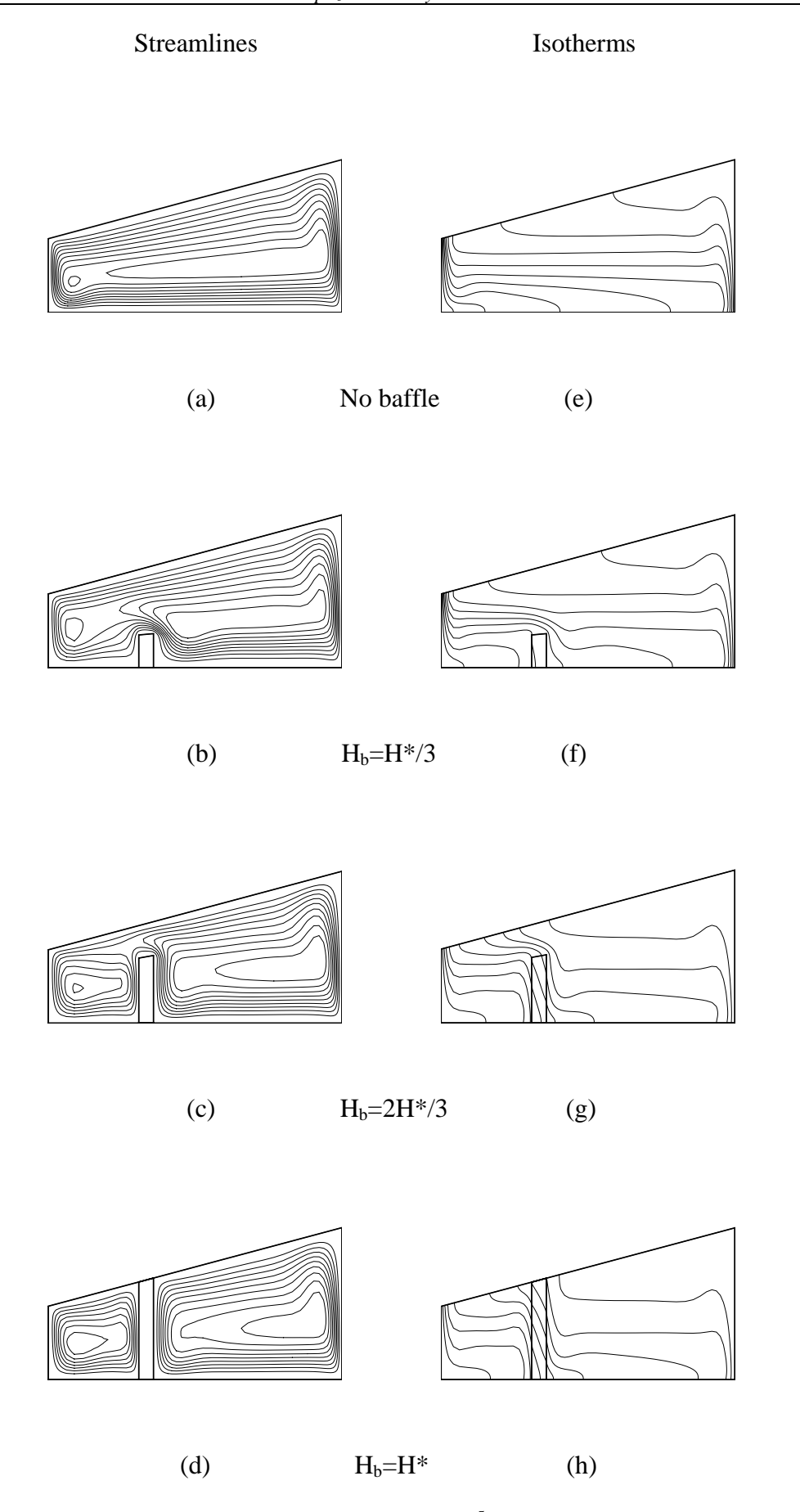
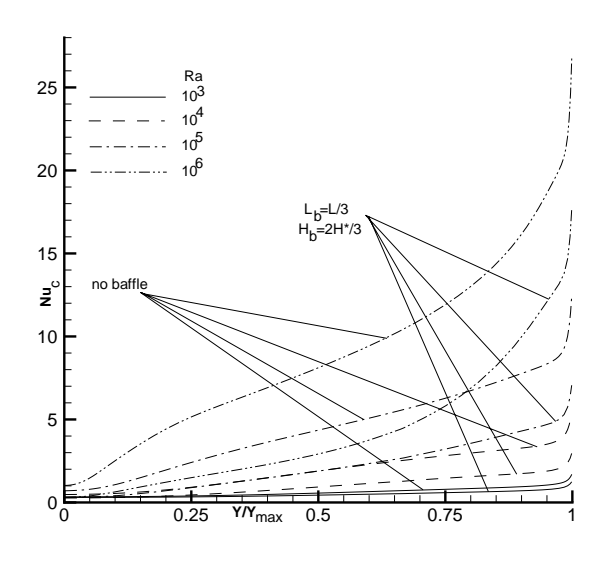
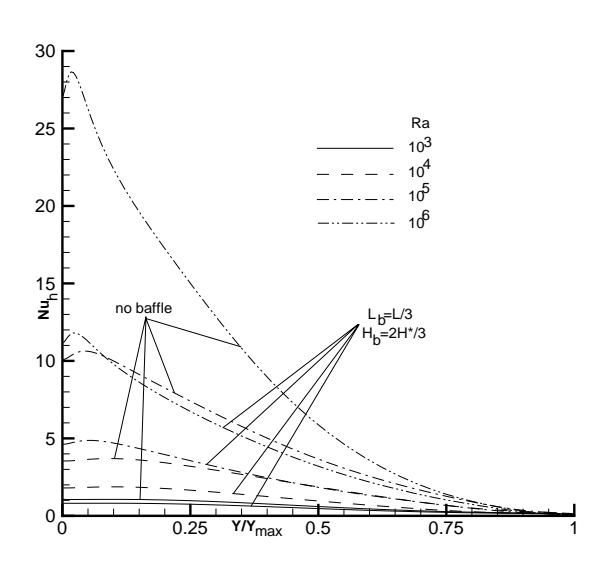


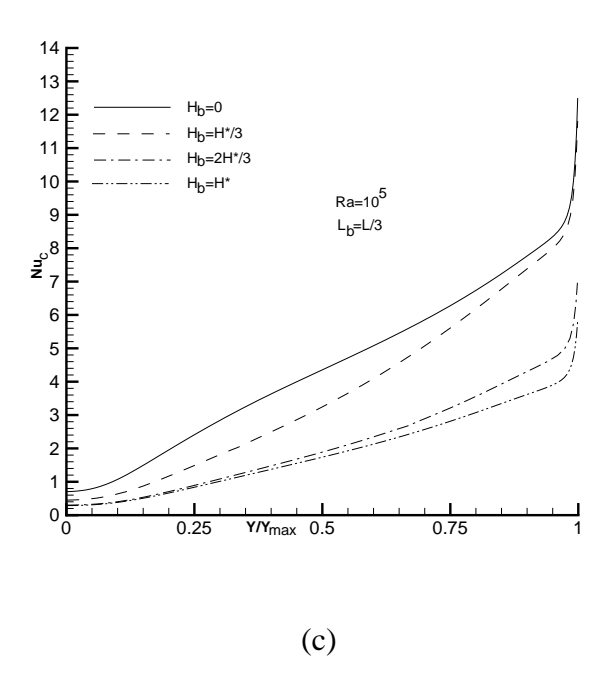
Fig. 10 Streamline and isotherm plots (Ra= 10^5 , L_b =L/3) at different H_b for the buoyancy opposing boundary condition



(a)



(b)



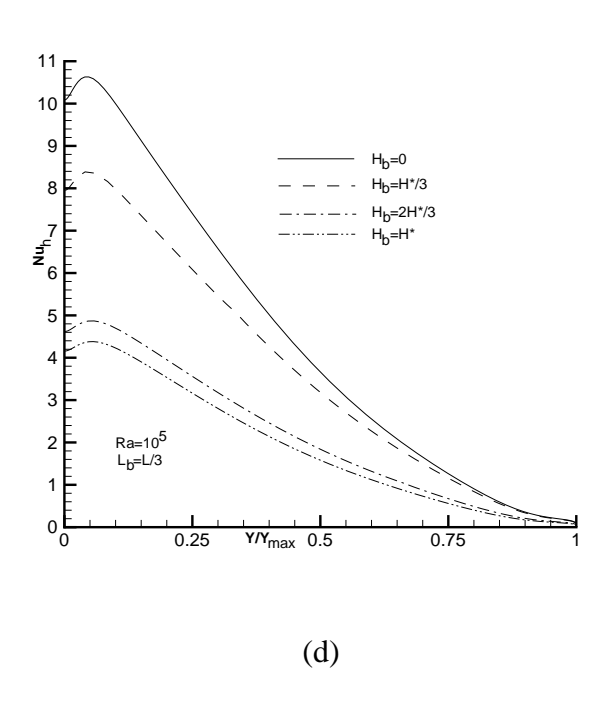


Fig. 11 Local Nusselt number distribution along (a,c) the hot and (b,d) cold walls for the buoyancy opposing boundary condition.